

# Direct identification of monolayer rhenium diselenide by an individual diffraction pattern

Zhen Fei<sup>1</sup>, Ching-Hwa Ho<sup>2</sup>, Fang Lin<sup>3</sup>, Jun Yuan<sup>4,1</sup>, Ze Zhang<sup>1</sup> and Chuanhong Jin<sup>1</sup> (✉)

<sup>1</sup> State Key Laboratory of Silicon Materials, School of Materials Science and Engineering, Zhejiang University, Hangzhou, 310027, China

<sup>2</sup> Graduate Institute of Applied Science and Technology, National Taiwan University of Science and Technology, Taipei 106, Taiwan

<sup>3</sup> College of Electronic Engineering, South China Agricultural University, Guangzhou, Guangdong 510642, China

<sup>4</sup> Department of Physics, University of York, Heslington, York YO10 5DD, UK

## ABSTRACT

In the current extensive studies of transition metal dichalcogenides (TMDCs), compared to hexagonal layered materials, like graphene, hBN and MoS<sub>2</sub>, low symmetry layered 2D crystals showed great potential for applications in anisotropic devices. Rhenium diselenide (ReSe<sub>2</sub>) has the bulk space group  $P\bar{1}$  and belongs to triclinic crystal system with a deformed cadmium iodide type structure. Here we unambiguously determined monolayer and its vertical orientation of rhenium diselenide membrane with an individual electron diffraction pattern, which could be applicable to low symmetry crystal systems, including both triclinic and monoclinic lattices, as long as their third unit-cell basis vector is not perpendicular to basal plane. Atomically resolved image from probe corrected annular dark field scanning transmission electron microscope (ADF-STEM) was employed to validate layer number. Finally, experimental results were well explained by kinematical electron diffraction theory and corresponding simulations.

## 1 Introduction

Since the celebrated fabrication of atomically thin carbon film field effect transistor, there have been a growing interest in investigating van der Waals layered materials among research communities[1]. Beyond graphene, especially in the family of transition metal dichalcogenides, when reduced to atomic thicknesses, they show great potential for future applications in semiconducting electronics and optoelectronics, and also open up more opportunities to explore novel physics phenomena in condensed matter physics, such as valley physics[2, 3], superconductivity[4], charge density waves[5, 6], and large magnetoresistance[7].

Of these materials, low symmetry 2D materials emerge as anisotropic electronic and optoelectronic candidates. Compared to graphene and MoS<sub>2</sub> with the highly symmetric hexagonal structures, those 2D materials with reduced symmetry, ranging from black

---

Address correspondence to Chuanhong Jin, chhjin@zju.edu.cn

phosphorus[8-10] and  $WTe_2$ [7] to  $ReS_2$  and  $ReSe_2$ , have internal anisotropic physical properties. Moreover,  $ReS_2$  and  $ReSe_2$  share similar crystal structures, they both have a distorted octahedral 1T structure and belong to triclinic crystal system, and Re atoms form zigzag chains in the basal plane, arising from the Peierls distortion. Therefore,  $ReSe_2$  and  $ReS_2$  flakes have both in-plane and out-of-plane anisotropy, and there are numbers of applications based on their anisotropic properties recently[11-16].

When materials are thinned down to atomically thin membranes, thickness begins to play an important role in tailoring their properties, and vice versa, there are a variety of techniques to determine their thicknesses, ranging from image contrast of reflected light microscopy[17-23], second harmonic microscopy[24-27], atomic force microscopy, cross-sectional imaging, as well as Raman and photoluminescence spectroscopy[28-31]. In the field of electron microscopy, there are miscellaneous methods to identify thickness as well, which includes peak shift in plasmon spectroscopy[32, 33], direct high-resolution transmission electron microscopy (HRTEM) imaging combined with simulation[34] and linearity in ADF-STEM signals[35, 36]. Among the above methods, spectroscopic analysis requires dedicated electron energy loss spectroscopy (EELS) detector and high brightness electron source, and thus limits its use for thickness characterizations. Also direct HRTEM imaging is often conducted in a microscope equipped with costly hard-ware aberration correctors and followed by a series of extended simulation processing, which limit the accessibility of these techniques. Intensities in ADF-STEM images could be used for determining relative thicknesses. In contrast to these methods, electron diffraction analysis[33, 37-42] could be conducted on any commercial uncorrected TEM conveniently with negligible beam damages on pristine crystalline samples compared to the former methods. Furthermore, in the previous reports on determining the thickness of 2D materials through electron diffraction[33, 37-42], they involve a series of sample tilting, here we demonstrate a method of identifying monolayer  $ReSe_2$  and its vertical orientation with one single diffraction pattern.

## 2 Theoretical basis

To illustrate the essence of electron diffraction evolution with thickness of atomically thin rhenium diselenide, an analytic kinematical diffraction theory approximation was developed in this study, which is usually applicable to ultra-thin specimens and light-element atoms. In the classic description of electron diffraction process, the electrons are scattered by specimen's electrostatic potential, and according to the first Born approximation, the amplitude of diffracted beam is proportional to the Fourier transform of the corresponding specimen's potential. Furthermore, without considering the effect of interatomic bonding, the total specimen's potential can be written as a superposition of all individual atoms' potentials and the Fourier transform of one atom's potential is its atomic scattering factor.

In the case of few-layer  $ReSe_2$ , we first take summations of atomic scattering factors over a unit cell, containing four rhenium and eight selenium atoms as shown in Fig. 1(a)&(b), then combine all unit cells along the thickness direction, which, as a whole, are defined as a basis sum term. Then we sum this term laterally over the entire basal plane, defined as two-dimensional lattice summation term. This is formulated as

$$f(\vec{K}) = \sum_{lattice} e^{-i2\pi\vec{K}\cdot\vec{R}_l} \sum_{basis} e^{-i2\pi\vec{K}\cdot\vec{R}_b} f_{atom(Re,Se)}(\vec{K}) \quad (1)$$

where  $R_l$  and  $R_b$  are the discrete lattice and basis vectors of the crystal respectively[37, 43, 44], which can be further simplified as

$$f(\vec{K}) = s_{lattice}(\vec{K})s_{stacking}(\vec{K})F_{structure}(\vec{K}) \quad (2)$$

We will discuss in detail about the multiplication of the three terms. The first term is the result of in-plane periodicity, by taking square of the modulus, we will have

$$|s_{lattice}(\vec{K})|^2 = \frac{\sin^2(\frac{n_1 2\pi\vec{K}\cdot\vec{a}}{2})\sin^2(\frac{n_2 2\pi\vec{K}\cdot\vec{b}}{2})}{\sin^2(\frac{2\pi\vec{K}\cdot\vec{a}}{2})\sin^2(\frac{2\pi\vec{K}\cdot\vec{b}}{2})} \quad (3)$$

where  $\vec{a}$  and  $\vec{b}$  are in-plane lattice vectors indicated in Fig. 1(a)&(b),  $n_1$  and  $n_2$  are the number of unit cells along their corresponding directions. This equation can be treated as a Dirac delta function,  $|s_{lattice}(\vec{K})|^2 \sim n_1 n_2 \delta(\alpha)\delta(\beta)$  as long as  $n_1$  and  $n_2$  are large, in other words, the illuminated area is large enough.  $\alpha$  and  $\beta$  represent deviation from reciprocal lattice points projected onto the in-plane directions, respectively. Therefore, this term is none-zero only for  $\vec{K} = \vec{G} + \vec{k}_\perp$ , where  $\vec{G} = h\vec{a}^* + k\vec{b}^* + l\vec{c}^*$ , representing the reciprocal lattice points, and  $\vec{k}_\perp$  is the perpendicular component of the vector describing deviation from the reciprocal lattice point. The second term is determined by how unit cells are stacked in the out-of-plane direction, expressed as

$$|s_{stacking}(\vec{K})|^2 = \frac{\sin^2(\frac{2\pi N\vec{K}\cdot\vec{c}}{2})}{\sin^2(\frac{2\pi\vec{K}\cdot\vec{c}}{2})} \quad (4)$$

which is similar to the first term, but only small number of  $N$  layers in the thickness direction, is considered. Therefore the value of the second term, also defined as the shape factor in conventional bulk crystal, will oscillate along the  $z$  direction, with the periodicity of  $c_z$ , the projection of  $\vec{c}$  onto  $z$  axis, as illustrated in Fig. 1(c), but stay constant for monolayer. The last term is named as the structure factor, by simply summing up all atomic factors in one unit cell, which can be calculated numerically according to the inversion symmetry inside the unit cell, then

$$|F_{structure}(\vec{K})|^2 = 4[f_{Re}(\vec{K}) \sum_{i=1}^2 \cos 2\pi(h\Delta a_i + k\Delta b_i + l\Delta c_i) + f_{Se}(\vec{K}) \sum_{j=1}^4 \cos 2\pi(h\Delta a_j + k\Delta b_j + l\Delta c_j)]^2 \quad (5)$$

Where  $\Delta a_i$ ,  $\Delta b_i$  and  $\Delta c_i$  represent Re atom's relative coordinate deviations from the unit cell center in the direction of  $\vec{a}$ ,  $\vec{b}$  and  $\vec{c}$  respectively, and there are two crystallographically inequivalent Re atom, the same rule can be applied to Se atoms.

To sum up, the first term restricts none-zero values to the rods in the reciprocal space, which

are located at the reciprocal lattice points and in perpendicular to the basal plane, then the shape factor modulates the intensity along the thickness direction, with a characteristic length of  $c_z$ , finally the structure factor tends to tune the intensity much more slowly in  $z$  direction, and thus modify the reciprocal rods at different  $(h, k)$  points in-plane. Note that we are mainly focusing on the shape factor, an indicator of the sample thickness. In Fig. 1(d), the shape factor of a bi-layer sample is visualized in the reciprocal space. More specifically, Figure. 1(e) shows a cross section of the shape factors of a pair of crystallographically equivalent in Fig. 1(d) and the intersection between the Ewald sphere and those reciprocal rods. Note that the two intersecting points are not symmetrical, and the distance between the intersection and centroid of the shape factor are written as  $\Delta_1$  and  $\Delta_2$  for the left and right rods respectively, which should be attributed to the curvature of the Ewald sphere and the oblique nature of  $a^*$  and  $b^*$  reciprocal basis vectors in the triclinic crystal lattice when the incident electron beam is in perpendicular to the basal plane. In other words, when the electron beam is perpendicular to the basal plane, the ReSe<sub>2</sub> crystal will not sit in the zone axis direction, and thus prerequisite of the well-known Friedel law cannot be satisfied, hence, there is a mismatch in intensity for a pair of crystallographically equivalent spots except for monolayer. In conclusion, the mismatch between a pair of spots can be used to unambiguously identify monolayer ReSe<sub>2</sub> crystalline with one single diffraction pattern.

### 3 Results and discussion

With the as-prepared sample, monolayer was first identified by atomic resolved ADF-STEM image, as a reference to demonstrate our following diffraction method. In Figure. 2(a), atoms of rhenium and selenide can be clearly resolved, and brighter atoms represent rhenium atoms since atom with higher atomic number scatters electrons more strongly. In the left side of this figure, diamond-shaped-chains are distinctively distinguishable, corresponding to the projection of monolayer atom structures, indicated by blue sphere model superimposed on these atom sites (inset is the low magnification ADF-STEM image). However, as layer number go up to two and more, the characteristic diamond-shaped-chains will disappear, and therefore, this feature could be used to test whether the region of interest is monolayer. Once the monolayer region is confirmed, using the relative intensity extracted from intensity profiles across various regions acquired under the same imaging condition, different thicknesses could be identified according to the step-like intensity profiles, as shown in Fig. 2(b). Thus, this method is employed to cross check thickness of few-layer ReSe<sub>2</sub> membranes.

Following the kinematic theory developed previously, we implemented MATLAB codes to simulate the diffraction intensity for ReSe<sub>2</sub> of different thicknesses, which are in comparison with the corresponding experimental ones. Simulated and experimental diffraction patterns are shown in Fig. 3(a)-(d) and (e)-(h) respectively, by inspecting, the geometry of the diffraction pattern is the projection of the reciprocal rods onto basal plane, and they form a quasi-equilateral triangular 2 dimensional lattice with minor modifications on both lateral lengths and angles. In addition, the brightest '6-fold' spots construct a quasi-hexagon in the middle (highlighted by a yellow hexagon in Fig. 3(d)), which is the direct result of structure factor, and the areas of the spots are defined as proportional to their intensities in the simulated results.

As the layer number increases, shape factor will be further modulated in the way described in Fig. 1(c), as well as those intersections of reciprocal rods and Ewald sphere, and as a result, some spots will go brighter while others go dimmer. Most importantly, except for monolayer, there will be a mismatch in intensity measurements for a pair of crystallographically equivalent diffraction spots, which is the fingerprint to distinguish monolayer ReSe<sub>2</sub>. In Figure. 3(i), the intensity mismatch varies with different layer numbers, and both simulated and experimental data show the same trend in intensity mismatch as layer number increases. However, experimental data tend to have larger error distribution at larger layer number, also their values are always higher than simulated ones, which should be attributed to dynamical scattering effects since both Re and Se are heavy atoms. In conclusion, by measuring the intensity difference between a pair of crystallographically equivalent diffraction spots, we can distinguish monolayer and multi-layer ReSe<sub>2</sub> membranes.

ReSe<sub>2</sub> belongs to triclinic crystal system, which has the lowest symmetry of all, and lacks the symmetry of C<sub>2</sub>, in other words, flipping ReSe<sub>2</sub> membrane over is not crystallographically equivalent, and such a character was found in diffraction pattern. In Figure. 4(a)&(b), there are diffraction patterns of the same chosen monolayer region with opposed vertical orientations (the chosen area are shown in their corresponding insets). We choose the brightest '6-fold' spots for quantitative intensity analysis, and draw a direction from the maxima to the minima, as indicated by an arc yellow arrow, and the direction will be reversed from clockwise to anticlockwise once the sample is flipped upside down. As illustrated in Fig. 4(c)&(d), at the original setting, intensities of the six spots are represented by different letters, and A>B>C, therefore, the arrow runs from A to C. Once the membrane is flipped along AA', their intensities change in the way shown in Fig. 4(d), and thus the direction shifts from clockwise to anticlockwise. Therefore this method can also be used to identify vertical direction.

*Generally, inspired by the method of tilt-series diffraction analysis to determine thickness of atomically thin crystals, we took advantage of the intrinsic low symmetry property of ReSe<sub>2</sub> crystal structure, and acquired an individual diffraction pattern containing the information of intensity mismatch of a pair of crystallographically equivalent spots, to identify monolayer. Furthermore, by quantitatively analyzing the intensities of the brightest '6-fold' spots from the monolayer, we also demonstrated that the in-plane direction of their intensity variation could be utilized to determine its vertical orientation, which could be exploited to anisotropic applications. More importantly, this method could be easily generalized to other 2D materials with triclinic or monoclinic lattice structures.*

## **4 Conclusions**

We conclude that by quantitatively analyzing electron diffraction pattern of few-layer ReSe<sub>2</sub> membranes, it is possible to identify monolayer and its vertical orientation without taking tilt series diffraction patterns, as previous reported thickness determination method by electron diffraction. In our study, we distinguish monolayer according to intensity mismatch of a pair of crystallographically equivalent diffraction spots, and determine its vertical orientation through the intensity variation direction of a couple of chosen diffraction spots. This analytical technique is based on the low symmetry in ReSe<sub>2</sub> crystal structure, and could be applicable to crystals of both triclinic system and monoclinic system, as long as their third unit-cell basis vector is not perpendicular to basal plane.

## Methods

Layered crystals of ReSe<sub>2</sub> were grown by chemical-vapor transport method using I<sub>2</sub> as the transport agent. The method consisted of two steps: First, prior to the crystal growth the powdered compound of the rhenium diselenide was prepared from the elements (Re: 99.95% and Se: 99.999%) by reaction at 1030 °C for 10 days in evacuated quartz ampoules. About 10 g of the elements were introduced into a quartz ampoule (19mm OD, 14mm ID, 15 cm length), which was then evacuated to about 10<sup>-6</sup> Torr and sealed. For crystal growth, the chemical transport was achieved by an appropriate amount (~10 g) of synthesized compound together with the transport agent (I<sub>2</sub> about 10 mg/cm<sup>3</sup>) placed in a quartz ampoule (22mm OD, 17mm ID, and 20 cm in length), which was then cooled with liquid nitrogen, evacuated to 10<sup>-6</sup> Torr and sealed. The quartz tube was then placed in a horizontal three-zone furnace and the charge pre-reacted for 24 h at 800 °C while the temperature of the growth zone was set at 1000 °C to prevent the transport of the product. The furnace was slowly set to give a constant temperature of 1000 °C across the reaction tube, and then programmed over 24 h to produce the temperature gradient at which single crystal growth takes place. Best results were obtained with temperature setting of about 1060→1010 °C in a temperature gradient of about -2.5 °C/cm and growth time of about 20 days.

To prepare free-standing few-layer ReSe<sub>2</sub> membranes, polydimethylsiloxane (PDMS) was used for micromechanical exfoliation of bulk high quality ReSe<sub>2</sub> crystals, and then thin flakes were deposited on top of an oxidized silicon wafer. Later, few-layer membranes were identified by optical microscope and the desired region was carefully aligned to holes of a lacey carbon TEM grid. Then, acetone was used to join carbon film and sample through evaporation of acetone in air, subsequently, NaOH solution was used to etch away the underneath SiO<sub>2</sub> layer. Finally, the TEM grid with sample on it was immersed in water to dissolve residual NaOH solute, and then acetone to prevent support film from rupturing, after dried in air, our sample is ready for further characterization.

Diffraction patterns of specimen were recorded on a FEI Tecnai G-F20 microscope operated at 200 kV. The uniform lateral dimension of few-layer membrane is on the scale of few microns, therefore an illuminated area of 200 nm in diameter was chosen by selected area aperture, to ensure electrons are from the region of interest. To obtain diffractions of the specimen with opposed vertical directions, the TEM grid was reloaded and flipped over outside the microscope. For quantitative diffraction intensity analysis, the exposure time was limited in the range where the response function of CCD detector remain linear.

The ADF-STEM images were recorded on a probe-corrected Titan ChemiSTEM at an acceleration voltage of 200 kV. After acquiring the atomic resolved images, we further processed images by a technique of superimposing a stack of drift corrected images to enhance signal to noise ratio for better visibility, hence, monolayer and multi-layer membranes can be unambiguously distinguished, more specifically, the multilayers are stacked with a lateral shift in basal plane, and the in-plane motif of diamond-shaped-chains for monolayer will be blurred when layer number increases. In addition, intensity profiles extracted from low-magnification

ADF-STEM image could be employed to determine the corresponding relative thickness, since the number of large-angle scattered electrons is approximately proportional to the number of atoms involved.

## Acknowledgements

This work is financially supported by the National Basic Research Program of China (Grant No. 2014CB932500 and No. 2015CB921004), the National Natural Science Foundation of China (Grant No. 51472215, No. 51222202, No. 61571197 and No. 61172011) and the Ministry of Science and Technology, Taiwan (MOST 104-2112-M-011-002-MY3). J.Y. acknowledges supports from Pao Yu-Kong International Foundation for a Chair Professorship in ZJU. This work made use of the resources of the Center of Electron Microscopy of Zhejiang University.

## References

- [1] Novoselov, K. S.; Geim, A. K.; Morozov, S. V.; Jiang, D.; Zhang, Y.; Dubonos, S. V.; Grigorieva, I. V.; Firsov, A. A. Electric field effect in atomically thin carbon films. *Science* **2004**, *306*, 666-669.
- [2] Zeng, H.; Dai, J.; Yao, W.; Xiao, D.; Cui, X. Valley polarization in MoS<sub>2</sub> monolayers by optical pumping. *Nat. Nanotechnol.* **2012**, *7*, 490-493.
- [3] Xiao, D.; Liu, G.-B.; Feng, W.; Xu, X.; Yao, W. Coupled spin and valley physics in monolayers of MoS<sub>2</sub> and other group-VI dichalcogenides. *Phys. Rev. Lett.* **2012**, *108*, 196802.
- [4] Sipos, B.; Kusmartseva, A. F.; Akrap, A.; Berger, H.; Forró, L.; Tutiš, E. From Mott state to superconductivity in 1T-TaS<sub>2</sub>. *Nat. Mater.* **2008**, *7*, 960-965.
- [5] Rossnagel, K. On the origin of charge-density waves in select layered transition-metal dichalcogenides. *J. Phys. Condens. Matter* **2011**, *23*, 213001.
- [6] Neto, A. C. Charge density wave, superconductivity, and anomalous metallic behavior in 2D transition metal dichalcogenides. *Phys. Rev. Lett.* **2001**, *86*, 4382.
- [7] Ali, M. N.; Xiong, J.; Flynn, S.; Tao, J.; Gibson, Q. D.; Schoop, L. M.; Liang, T.; Haldolaarachchige, N.; Hirschberger, M.; Ong, N. Large, non-saturating magnetoresistance in WTe<sub>2</sub>. *Nature* **2014**, *514*, 205-208.
- [8] Ribeiro, H. B.; Pimenta, M. A.; de Matos, C. J.; Moreira, R. L.; Rodin, A. S.; Zapata, J. D.; de Souza, E. A.; Castro Neto, A. H. Unusual angular dependence of the Raman response in black phosphorus. *ACS Nano* **2015**, *9*, 4270-4276.
- [9] Lu, W.; Ma, X.; Fei, Z.; Zhou, J.; Zhang, Z.; Jin, C.; Zhang, Z. Probing the anisotropic behaviors of black phosphorus by transmission electron microscopy, angular-dependent Raman spectra, and electronic transport measurements. *Applied Physics Letters* **2015**, *107*, 021906.
- [10] Xia, F.; Wang, H.; Jia, Y. Rediscovering black phosphorus as an anisotropic layered material for optoelectronics and electronics. *Nature Communications* **2014**, *5*.
- [11] Chenet, D. A.; Aslan, O. B.; Huang, P. Y.; Fan, C.; van der Zande, A. M.; Heinz, T. F.; Hone, J. C. In-plane anisotropy in mono- and few-layer ReS<sub>2</sub> probed by Raman spectroscopy and scanning transmission electron microscopy. *Nano Lett.* **2015**, *15*, 5667-5672.
- [12] Liu, E.; Fu, Y.; Wang, Y.; Feng, Y.; Liu, H.; Wan, X.; Zhou, W.; Wang, B.; Shao, L.; Ho, C.-H. Integrated digital inverters based on two-dimensional anisotropic ReS<sub>2</sub> field-effect transistors. *Nat. Commun.* **2015**, *6*, 6991
- [13] Zhong, H.-X.; Gao, S.; Shi, J.-J.; Yang, L. Quasiparticle band gaps, excitonic effects, and anisotropic optical

- properties of the monolayer distorted 1T diamond-chain structures ReS<sub>2</sub> and ReSe<sub>2</sub>. *Phys. Rev. B* **2015**, *92*, 115438.
- [14] Wolverson, D.; Crampin, S.; Kazemi, A. S.; Ilie, A.; Bending, S. J. Raman spectra of monolayer, few-layer, and bulk ReSe<sub>2</sub>: An anisotropic layered semiconductor. *ACS Nano* **2014**, *8*, 11154-11164.
- [15] Hart, L.; Dale, S.; Hoyer, S.; Webb, J. L.; Wolverson, D. Rhenium dichalcogenides: layered semiconductors with two vertical orientations. *Nano Lett.* **2016**, *16*, 1381-1386.
- [16] Lin, Y.-C.; Komsa, H.-P.; Yeh, C.-H.; Björkman, T. r.; Liang, Z.-Y.; Ho, C.-H.; Huang, Y.-S.; Chiu, P.-W.; Krasheninnikov, A. V.; Suenaga, K. Single-layer ReS<sub>2</sub>: two-dimensional semiconductor with tunable in-plane anisotropy. *ACS Nano* **2015**, *9*, 11249-11257.
- [17] Abergel, D.; Russell, A.; Fal'ko, V. I. Visibility of graphene flakes on a dielectric substrate. *arXiv preprint arXiv:0705.0091* **2007**.
- [18] Benameur, M.; Radisavljevic, B.; Heron, J.; Sahoo, S.; Berger, H.; Kis, A. Visibility of dichalcogenide nanolayers. *Nanotechnology* **2011**, *22*, 125706.
- [19] Jung, I.; Pelton, M.; Piner, R.; Dikin, D. A.; Stankovich, S.; Watcharotone, S.; Hausner, M.; Ruoff, R. S. Simple approach for high-contrast optical imaging and characterization of graphene-based sheets. *Nano Lett.* **2007**, *7*, 3569-3575.
- [20] Casiraghi, C.; Hartschuh, A.; Lidorikis, E.; Qian, H.; Harutyunyan, H.; Gokus, T.; Novoselov, K.; Ferrari, A. Rayleigh imaging of graphene and graphene layers. *Nano Lett.* **2007**, *7*, 2711-2717.
- [21] Li, H.; Lu, G.; Yin, Z.; He, Q.; Li, H.; Zhang, Q.; Zhang, H. Optical Identification of Single - and Few - Layer MoS<sub>2</sub> Sheets. *Small* **2012**, *8*, 682-686.
- [22] Blake, P.; Hill, E.; Neto, A. C.; Novoselov, K.; Jiang, D.; Yang, R.; Booth, T.; Geim, A. Making graphene visible. *Appl. Phys. Lett.* **2007**, *91*, 063124.
- [23] Ni, Z.; Wang, H.; Kasim, J.; Fan, H.; Yu, T.; Wu, Y.; Feng, Y.; Shen, Z. Graphene thickness determination using reflection and contrast spectroscopy. *Nano Lett.* **2007**, *7*, 2758-2763.
- [24] Yin, X.; Ye, Z.; Chenet, D. A.; Ye, Y.; O'Brien, K.; Hone, J. C.; Zhang, X. Edge nonlinear optics on a MoS<sub>2</sub> atomic monolayer. *Science* **2014**, *344*, 488-490.
- [25] Malard, L. M.; Alencar, T. V.; Barboza, A. P. M.; Mak, K. F.; de Paula, A. M. Observation of intense second harmonic generation from MoS<sub>2</sub> atomic crystals. *Phys. Rev. B* **2013**, *87*, 201401.
- [26] Zeng, H.; Liu, G.-B.; Dai, J.; Yan, Y.; Zhu, B.; He, R.; Xie, L.; Xu, S.; Chen, X.; Yao, W. Optical signature of symmetry variations and spin-valley coupling in atomically thin tungsten dichalcogenides. *Sci. Rep.* **2013**, *3*, 1608.
- [27] Kumar, N.; Najmaei, S.; Cui, Q.; Ceballos, F.; Ajayan, P. M.; Lou, J.; Zhao, H. Second harmonic microscopy of monolayer MoS<sub>2</sub>. *Phys. Rev. B* **2013**, *87*, 161403.
- [28] Mak, K. F.; Lee, C.; Hone, J.; Shan, J.; Heinz, T. F. Atomically thin MoS<sub>2</sub>: a new direct-gap semiconductor. *Phys. Rev. Lett.* **2010**, *105*, 136805.
- [29] Splendiani, A.; Sun, L.; Zhang, Y.; Li, T.; Kim, J.; Chim, C.-Y.; Galli, G.; Wang, F. Emerging photoluminescence in monolayer MoS<sub>2</sub>. *Nano Lett.* **2010**, *10*, 1271-1275.
- [30] Ferrari, A. C.; Basko, D. M. Raman spectroscopy as a versatile tool for studying the properties of graphene. *Nat. Nanotechnol.* **2013**, *8*, 235-246.
- [31] Ferrari, A.; Meyer, J.; Scardaci, V.; Casiraghi, C.; Lazzeri, M.; Mauri, F.; Piscanec, S.; Jiang, D.; Novoselov, K.; Roth, S. Raman spectrum of graphene and graphene layers. *Phys. Rev. Lett.* **2006**, *97*, 187401.
- [32] Politano, A.; Chiarello, G.; Spinella, C. Plasmon spectroscopy of graphene and other two-dimensional materials with transmission electron microscopy. *Materials Science in Semiconductor Processing* **2016**.
- [33] Pan, C.; Nair, R.; Bangert, U.; Ramasse, Q.; Jalil, R.; Zan, R.; Seabourne, C.; Scott, A. Nanoscale electron

- diffraction and plasmon spectroscopy of single- and few-layer boron nitride. *Phys. Rev. B* **2012**, *85*, 045440.
- [34] Wu, R. J.; Odlyzko, M. L.; Mkhoyan, K. A. Determining the thickness of atomically thin MoS<sub>2</sub> and WS<sub>2</sub> in the TEM. *Ultramicroscopy* **2014**, *147*, 8-20.
- [35] Yamashita, S.; Koshiya, S.; Ishizuka, K.; Kimoto, K. Quantitative annular dark-field imaging of single-layer graphene. *Microscopy* **2015**, 10.1093/jmicro/dfu115, dfu115.
- [36] Zhou, W.; Zou, X.; Najmaei, S.; Liu, Z.; Shi, Y.; Kong, J.; Lou, J.; Ajayan, P. M.; Yakobson, B. I.; Idrobo, J.-C. Intrinsic structural defects in monolayer molybdenum disulfide. *Nano letters* **2013**, *13*, 2615-2622.
- [37] Shevitski, B.; Mecklenburg, M.; Hubbard, W. A.; White, E.; Dawson, B.; Lodge, M.; Ishigami, M.; Regan, B. Dark-field transmission electron microscopy and the Debye-Waller factor of graphene. *Phys. Rev. B* **2013**, *87*, 045417.
- [38] Odlyzko, M. L.; Mkhoyan, K. A. Identifying hexagonal boron nitride monolayers by transmission electron microscopy. *Microscopy and Microanalysis* **2012**, *18*, 558-567.
- [39] Ping, J.; Fuhrer, M. S. Layer number and stacking sequence imaging of few-layer graphene by transmission electron microscopy. *Nano Lett.* **2012**, *12*, 4635-4641.
- [40] Meyer, J.; Geim, A.; Katsnelson, M.; Novoselov, K.; Obergfell, D.; Roth, S.; Girit, C.; Zettl, A. On the roughness of single- and bi-layer graphene membranes. *Solid State Commun.* **2007**, *143*, 101-109.
- [41] Kumar, P.; Agrawal, K. V.; Tsapatsis, M.; Mkhoyan, K. A. Quantification of thickness and wrinkling of exfoliated two-dimensional zeolite nanosheets. *Nat. Commun.* **2015**, *6*, 7128.
- [42] Brown, L.; Hovden, R.; Huang, P.; Wojcik, M.; Muller, D. A.; Park, J. Twinning and twisting of tri- and bilayer graphene. *Nano Lett.* **2012**, *12*, 1609-1615.
- [43] Reimer, L. *Transmission Electron Microscopy: Physics of Image Formation and Microanalysis*; Springer, 2013.
- [44] Wang, Z.-l. *Elastic and Inelastic Scattering in Electron Diffraction and Imaging*; Springer Science & Business Media, 2013.

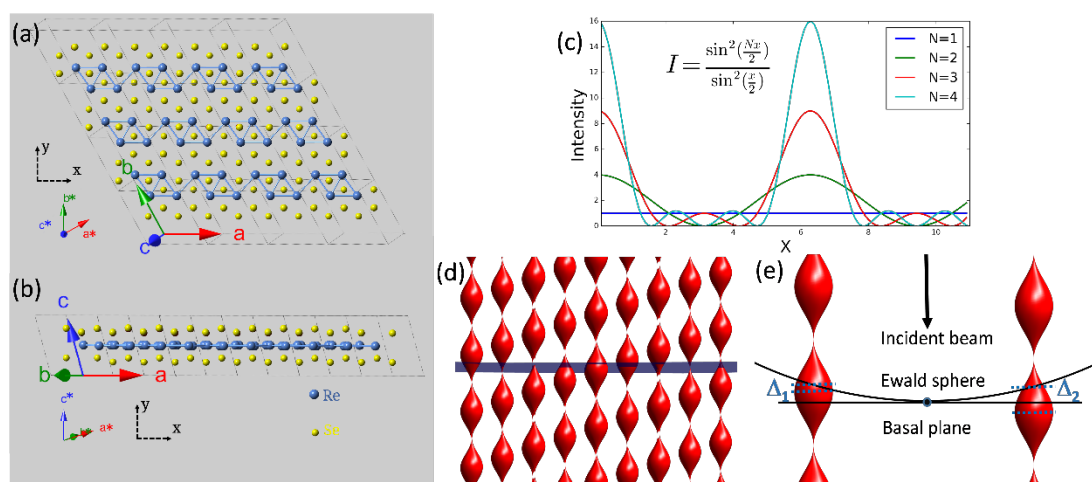


**Figure 1** Structure of ReSe<sub>2</sub> in direct and reciprocal space: (a) Atomic structure viewed from z-direction in Cartesian coordinates, unit cell basis vectors are coded with different colors, and reciprocal unit cell basis vectors are marked by superscripts stars. (b) Atomic structure viewed from y-direction. (c) Shape factor modulation for different thicknesses. (d) Visualization of shape factors in reciprocal space for the bi-layer ReSe<sub>2</sub> crystalline. (e) Schematic description of the asymmetrical intersection between a pair of crystallographically equivalent shape factors and Ewald sphere.

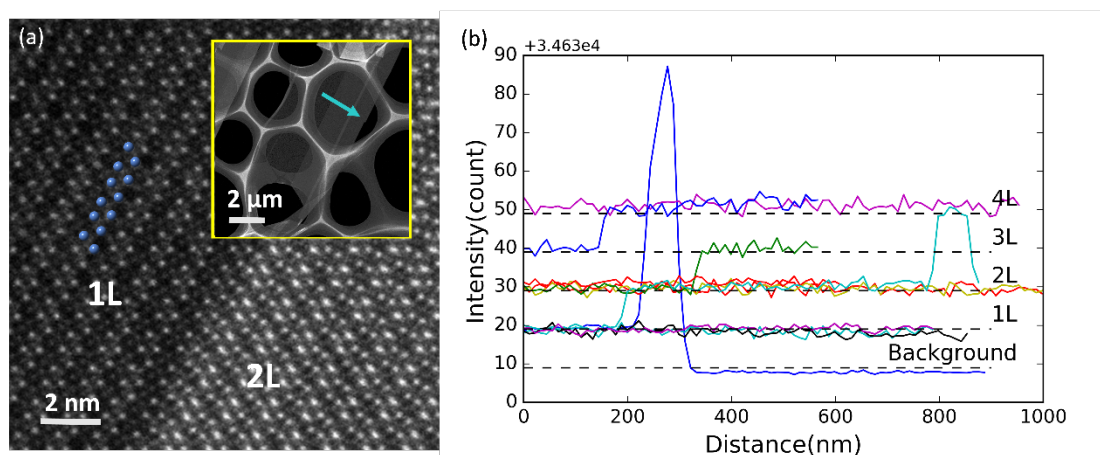


**Figure 2** (a) Atomically resolved image of monolayer and bilayer ReSe<sub>2</sub>, inset is the corresponding low-magnification ADF-STEM image. (b) Step-like intensity profiles for different thicknesses, the greenish line is extracted along the greenish arrow in (a) inset.

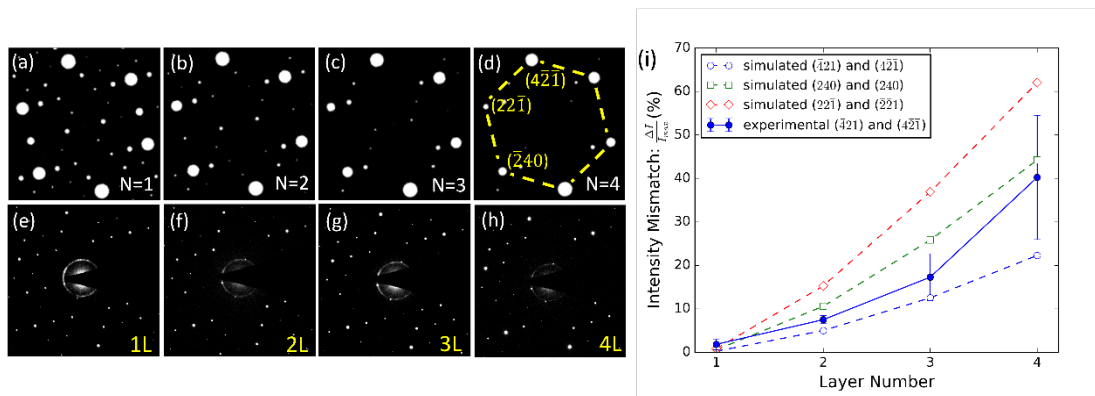


**Figure 3** (a)-(d) Simulated diffraction patterns for 1,2,3,4-layer ReSe<sub>2</sub> respectively. (e)-(h) Experimental results of diffraction for the corresponding thickness. (i) Intensity mismatch of the chosen crystallographically equivalent diffraction spot pairs, varying with layer number.

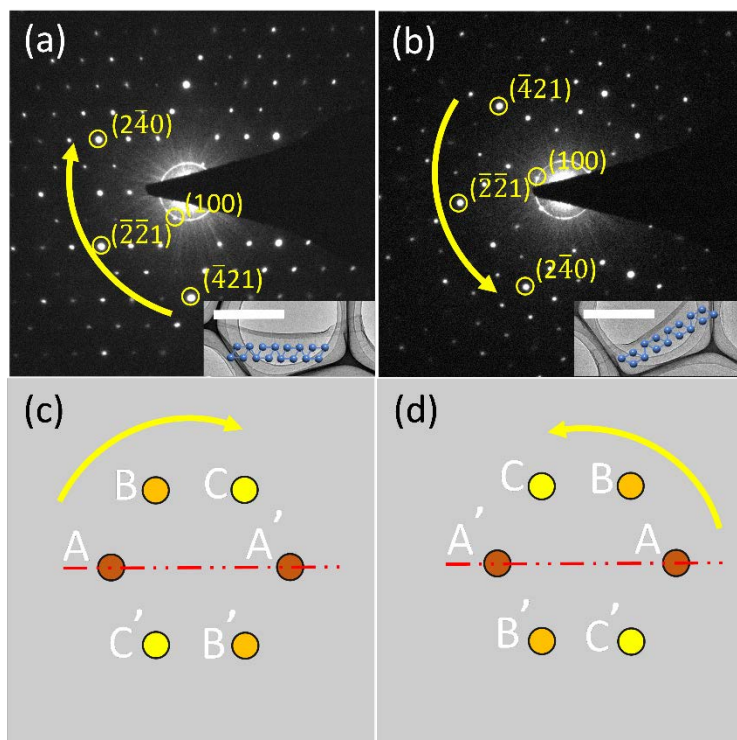


**Figure 4** (a)&(b) Electron diffraction and corresponding TEM image for upside orientated monolayer ReSe<sub>2</sub>, the yellow curved arrow indicated descending direction in intensity for the specified spots. Insets are their corresponding direct space images, scale bar is 1  $\mu$ m. (c)&(d) Schematic description of how intensities of electron diffraction spots vary when thin ReSe<sub>2</sub> flake is flipped over along axis AA', notice the relation  $A > B > C$ , as indicated by the yellow arrow, same as  $A', B', C'$ .